Ante- and post-mortem cellular injury dynamics in hybrid poplar foliage as a function of phytotoxic O3 dose

Benjamin Turc, Yves Jolivet, Mireille Cabané, Marcus Schaub, Pierre Vollenweider

HAL Id: hal-04327097
https://hal.inrae.fr/hal-04327097

Submitted on 28 Feb 2024

RESEARCH ARTICLE

Ante- and *post-mortem* cellular injury dynamics in hybrid poplar foliage as a function of phytotoxic O_3 dose

Benjamin Turc [1,2]*, **Yves Jolivet**[1], **Mireille Cabané**[1], **Marcus Schaub**[2], **Pierre Vollenweider**[2]

1 UMR Silva, AgroParisTech, INRAE, University of Lorraine, Lorraine, France, **2** Swiss Federal Institute for Forest, Snow and Landscape Research WSL, Birmensdorf, Switzerland

* bturc2@unl.edu

Abstract

After reaching phytotoxic levels during the last century, tropospheric ozone (O_3) pollution is likely to remain a major concern in the coming decades. Despite similar injury processes, there is astounding interspecific–and sometimes intraspecific–foliar symptom variability, which may be related to spatial and temporal variation in injury dynamics. After characterizing the dynamics of physiological responses and O_3 injury in the foliage of hybrid poplar in an earlier study, here we investigated the dynamics of changes in the cell structure occurring in the mesophyll as a function of O_3 treatment, time, phytotoxic O_3 dose (POD_0), leaf developmental stage, and mesophyll layer. While the number of Hypersensitive Response-like (HR-like) lesions increased with higher O_3 concentrations and POD_0, especially in older leaves, most structural HR-like markers developed after cell death, independent of the experimental factors. The pace of degenerative Accelerated Cell Senescence (ACS) responses depended closely on the O_3 concentration and POD_0, in interaction with leaf age. Changes in total chlorophyll content, plastoglobuli and chloroplast shape pointed to thylakoid membranes in chloroplasts as being especially sensitive to O_3 stress. Hence, our study demonstrates that early HR-like markers can provide reasonably specific, sensitive and reliable quantitative structural estimates of O_3 stress for *e.g.* risk assessment studies, especially if they are associated with degenerative and thylakoid-related injury in chloroplasts from mesophyll.

Introduction

Tropospheric ozone (O_3) concentrations have increased during the past century, as a consequence of increasing NO_x and volatile organic compound (VOC) levels [1, 2]. Over the last decade, there has been a slight decrease in tropospheric O_3 levels in North America and Europe as a result of emission control [3, 4]. In contrast, ground-level concentrations of O_3 are still increasing in highly polluted Asian areas, due to progressing industrialization and urbanization [5–7]. As a consequence, crop yields decreased by 10–20%, depending on the species

[8–10], and biomass production of trees decreased by 15% [11–13], leading to significant economic loss [14]. O_3 uptake and its impact on plants are mediated by leaf conductance and the opening of stomata [15, 16]. Accordingly, critical O_3 levels (CLs) for preventing adverse effects such as yield or biomass loss are based on O_3 flux assessments and have been defined for several plant types and groups [17]. However, the relationship between such metrics and effective O_3 impacts on physiological and cellular processes has remained poorly defined and understood so far [18].

As hypothesized by Vollenweider, Günthardt-Goerg [19] on the basis of converging evidence [20–24], Turc, Vollenweider [18] recently demonstrated that the distinct responses to O_3 stress within leaf tissues develop according to specific dynamics. They further highlighted the importance of environmental conditions regarding O_3 responses, given the close dependency between response order and illumination conditions. Reaching the leaf apoplast, O_3 quickly breaks down, causing the formation of reactive oxygen species (ROS) and cascades of oxidative bursts [25, 26]. If a threshold within the mesophyll symplast is exceeded, oxidative stress triggers the formation of necrotic lesions, resulting from programmed cell death (PCD) events and termed hypersensitive response-like (HR-like) [18, 27, 28]. Within distinct cells–or preceding the development of HR-like lesions–higher levels of oxidative stress accelerate cell senescence (ACS response), with suites of structural symptoms closely mimicking those during autumnal senescence—another type of PCD [19, 29, 30]. However, the flux-based O_3 dose responsible for different types of cellular injuries and processes remains elusive. Furthermore, the dynamics of processes and structural injuries within cells are still poorly understood, missing the quantitative markers necessary for reproducible assessments, whereas the sequence of reactions appears to significantly determine the terminal symptom display [19]. The investigation of such processes is important for supporting the analysis of visible injury in foliage, a widely used indicator of O_3 stress in risk assessment [31–33] and monitoring studies [34, 35]. Furthermore, characterizing cellular responses can contribute to our understanding of oxidative stress traits, given the sometimes-confounding variability of symptoms, by directing our attention to symptom severity rather than visibility. Finally, such investigations can highlight the interplay with environmental conditions and specify the contribution of synergic environmental constraints to the display of visible symptoms [23, 24, 36].

The ontogenetic developmental stage of foliage also contributes to the O_3 stress response, as it is responsible for, e.g., characteristic gradients of visible symptoms within foliage in terms of distribution and frequency [37, 38]. A greater tolerance of younger *versus* older foliage at higher *versus* lower shoot position has been observed in the field and under controlled conditions, irrespective of the species and the environmental conditions [38–40]. For example, after eight days of exposure to 100 ppb O_3 ($POD_0 > 5$ mmol O_3 m^{-2}), Turc, Vollenweider [18] observed HR-like lesions on more than 6% percentage area in mature foliage *versus* less than 1%, in the case of expanding leaves. The mechanisms responsible for higher O_3 tolerance in younger foliage have remained rather elusive so far. Current evidence indicates that the observed tolerance is not caused by a lower O_3 uptake and dose [18, 39, 41]. The involvement of ROS during developmental processes such as cell expansion [42] or the senescence-like responses elicited by O_3 stress point to the significance of ontogenetic leaf development and ROS interactions regarding the dynamics of O_3 injury. However, O_3 injury assessments are performed almost exclusively on older foliage and evidence relating foliar ontogenetic development to the dynamics of O_3 injury is scarce.

After characterizing the early physiological and injury dynamics [18], the main objective of the present study was to deepen our understanding regarding the structural reactions to O_3 stress down to the cellular and subcellular level. Specifically, we analyzed the dynamics of structural and ultrastructural changes as a function of flux-based O_3 dose and leaf ontogenetic

development, testing the following hypotheses (H): (H1) structural injury develops in parallel with physiological and biochemical reactions; (H2) not only the structural markers but also their dynamics within mesophyll cells are response-specific; (H3) cellular reactions and ultra-structural markers of O_3 stress depend on ontogenetic leaf development; (H4) in the case of ACS responses and as a consequence of leaf ontogenetic development, time-based dynamics differ from flux-based dynamics. Response to O_3 stress were investigated in the framework of a replicated experiment with assessments in brightfield (LM), fluorescence (FM) and transmitted electron (TEM) microscopy. We used the same facility, plant material and exposure conditions as in Turc, Vollenweider [18] and we repeated the physiological and injury assessments completed in that study. Quantitative data used to characterize the dynamics of HR-like processes and ACS responses was obtained by means of a PCD assay [18] and biochemical measurements of chlorophyll content [43, 44]. In addition, chloroplast traits were assessed using TEM images and computer-assisted image analysis.

Materials and methods

Experimental setting

The experimental conditions, the tested material and the physiological and injury assessments are described in detail in Turc, Vollenweider [18]. Briefly, young hybrid poplar clones (*Populus tremula x alba*; INRAE 717-1b4) were micropropagated before growing for 1.5 months in a growth chamber (22˚C/18˚C day/night temperature and 75%/85% day/night relative humidity) with a 14 h photoperiod (Philips Son-T Agro 400 W lamps, PAR = 350 µmol m^{-2} s^{-1}). The O_3 exposure was carried out using 48 poplar trees distributed across six identical phytotron chambers (PEPLor platform, Faculty of Sciences and Technologies, University of Lorraine) with three O_3 treatments (charcoal-filtered (CF) air, CF + 80 ppb O_3 and CF + 100 ppb O_3) and two replications of each (n = 16 trees). All foliar assessments were repeated on four trees per treatment at the 3rd and 10th leaf position from the tree base i.e., the youngest fully expanded leaf and the youngest leaf still expanding by the start of exposure. Stomatal conductance to water vapor (g_w) was measured 3 h after starting O_3 exposure using a LI-6400 portable photosynthesis system (LiCor, Inc, Lincoln, NE, United States) and inside the phytotron chambers). Measurements of g_w were used to estimate cumulated O_3 uptake (POD$_0$; [18, 45].

Assessment of ACS dynamics

The dynamics of degenerative changes indicative of ACS responses were assessed, measuring the foliar chlorophyll content [43, 44]. Leaf halves without midvein at the 3rd and 10th leaf position were repeatedly sampled (2, 8, 13, 23 days of treatment) and immediately shock-frozen in liquid nitrogen. They were homogenized in the same medium and the chlorophylls were extracted, solubilizing 100 mg of the homogenates in 1 ml acetone and incubating the mixture 15 min in the dark at 4˚C, prior to centrifugation (10 000 rpm / 10 min / 4˚C). The retrieved supernatants were diluted with distilled water [4:1, (v/v)] and absorbances were read at 663.2 nm and 646.8 nm (SAFAS UVmc1 spectrophotometer). For each sample, the extraction was repeated until the measured absorbance felt close to the detection limit. The estimates were converted into total chlorophyll concentrations (*Chl$_{tot}$*; mg g^{-1} of FM) using the absorbance coefficients provided by Lichtenthaler [43]:

$$Chl_{tot} = 7.15 * A_{663.2} + 18.71 * A_{646.8}$$

The *Chl$_{tot}$* values for the sample aliquots were summed up.

Assessments of cellular injury and HR-like dynamics

Dynamics of HR-like lesions were assessed by means of Trypan Blue vital staining and computer-assisted image analysis [18]. Therefore, two 6 mm discs per leaf position in four trees per treatment were sampled after 2, 8, 13 and 23 days of exposure. In addition, two other leaf discs were excised on each sampling date for structural and histochemical investigations of HR-like and ACS responses and dynamics at the cellular and subcellular level. The discs were fixed using EM-grade 2.5% glutaraldehyde buffered at pH 7.0 with 0.067 M Soerensen phosphate buffer, renewed after vacuum infiltration, and stored at 4˚C until further processing.

For LM and FM investigations, samples were dehydrated with 2-methoxyethanol (three changes), ethanol, n-propanol and n-butanol [46], then embedded in Technovit 7100 resin (Kulzer HistoTechnik). 1.5 μm semi-thin sections were trimmed from the center of the sampled discs using a Reichert Supercut 2050 microtome. Preparations were stained with Toluidine blue for observing the tissue and cell structure; callose deposits were specifically revealed using Aniline blue [47]. All assessments were performed using the 5× to 100× objectives of a Leica Leitz DM/RB microscope, diascopic or epifluorescent (UV excitation with filter cube A) light and an imaging system consisting of an INFINITY 2-1R camera and the Lumenera Infinity Analyze (release 6.4) software (Lumenera Corp., Ottawa, ON, Canada).

For TEM investigations, leaf blade patches excised from the center of EM-grade fixed samples were post-fixed in buffered 2% OsO_4, dehydrated by successive baths of graded ethanol, infiltrated by a series of graded propylene oxide/Epon 812 mixtures (with DDSA, NMA, DMP hardener), and embedded in Epon. Ultra-thin sections (70 nm) were cut using a Reichert UltraCut S ultra-microtome, mounted on gold grids, and contrasted using saturated uranyl acetate in 50% ethanol and lead citrate (Reynold procedure). Sections were observed using a Philipps CM12 transmission electron microscope.

The dynamics of ACS-related injury were assessed by means of chloroplast trait measurements, as this organelle is particularly sensitive to oxidative stress and shows characteristic alterations during senescence processes [19, 48, 49]. Using TEM pictures (17500× magnification) and the ImageJ software (vers. 2.0.0; [50]), size (area/perimeter/long and short axis/area of plastoglobuli and starch grains) were assessed by applying computer-assisted image analysis. Chloroplast shape was estimated by calculating chloroplast circularity (Cir_{chloro}), following the formula:

$$Cir_{chloro} = \frac{A_{chloro} * 4\pi}{P_{chloro}{}^2}$$

where A_{chloro} and P_{chloro} are the chloroplast area and perimeter, respectively.

Measurements were repeated, selecting ten cross-sectioned chloroplasts within 3 to 4 cells per upper and lower palisade parenchyma layer within each sample. Together with chlorophyll data, the measured chloroplast traits were used to calculate conceptual models synthesizing the ultrastructural responses in chloroplasts in response to experimental factors. Elliptical representations of chloroplasts, accumulated starch grains and plastoglobuli percentage areas were drawn using the *Plotrix* package [51] of R software, version 3.5.0 [52].

Statistical analysis

The dynamics of injury, ultrastructural and physiological responses to experimental factors were analyzed using linear mixed effects (LME) models. The fixed-effect factors included the time or POD_0, O₃ treatment, leaf position, mesophyll layer (chloroplast ultrastructural data), and their interactions. The random-effect factors included the tree nested in the chamber (leaf data, with leaf position forming the statistical unit) and the cell nested in the tree (chloroplast

ultrastructural data, with chloroplast forming the statistical unit). All statistical analyses (LME models and post-hoc tests) were performed using the *lme4* [53] and *lsmeans* [54] R packages.
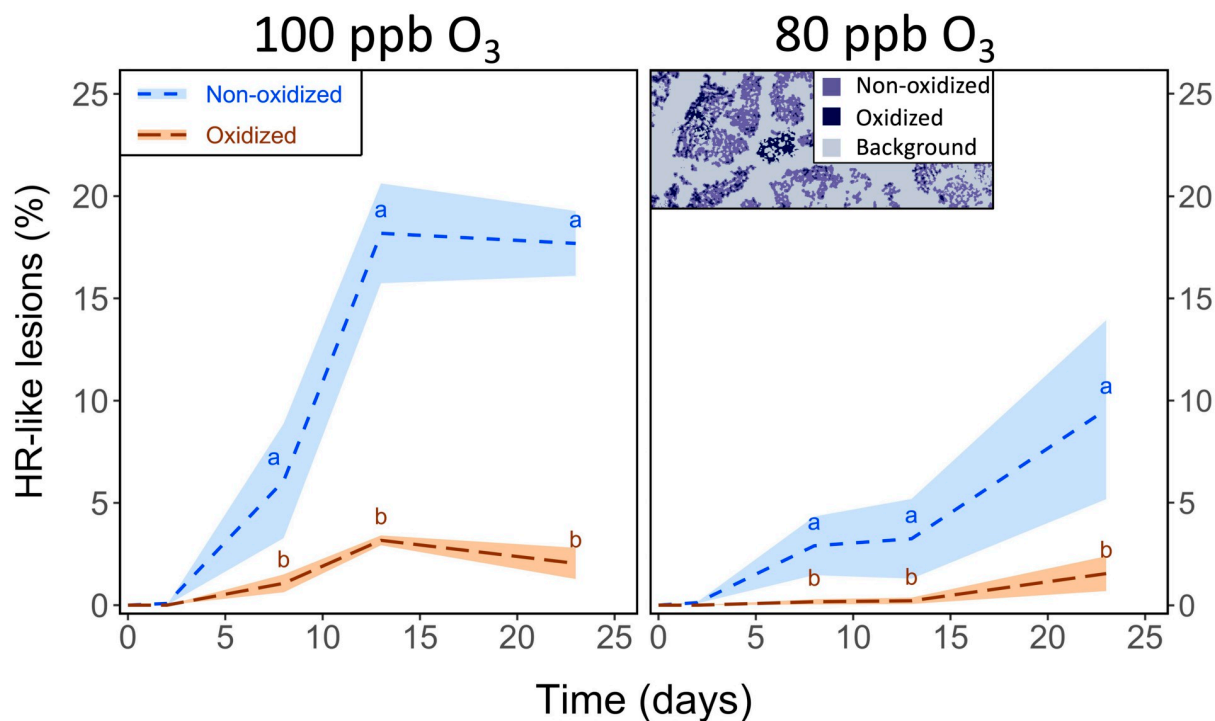
Results

Dynamics of leaf responses

In the 100 ppb O_3 treatment at both leaf positions (Fig 1, S1 Fig), the development of lesions (especially non-oxidized) showed a clear sigmoid-like dynamic. Despite rather synchronous dynamics, the leaf percentage area showing non-oxidized *versus* oxidized HR-like lesions was always greater, with the exceedance reaching an 8.4× order of magnitude at both leaf positions in the 100 ppb O_3 treatment by the end of the experiment (Fig 1 and S1 Fig; oxidation state: $P < 0.001$; oxidation state*time: $P < 0.001$). Differences between the 100 and 80 ppb O_3 treatment in the leaf percentage area showing non-oxidized and oxidized lesions at the two leaf positions became significant after 13 days of exposure (Fig 1 and S1 Fig). Similar but weaker injury and a delayed onset of HR-like processes were observed at the 10th *versus* the 3rd leaf position (S1 Fig *versus* Fig 1; O_3 treatment*leaf position: $P < 0.05$, O_3 treatment*time*leaf position: $P < 0.001$).

Also, in the case of chlorophyll measurements, the O_3 effects were generally more pronounced in the 100 *versus* 80 ppb O_3 treatment, with the chlorophyll decrease triggered by O_3 stress observed after 13 days of exposure (Fig 2A), and the O_3 treatment factor being then significant (O_3 treatment: $P < 0.001$, O_3 treatment*time: $P < 0.001$). Reported to the chlorophyll amounts in the CF treatment, the relative chlorophyll content in trees from the two O_3 treatments was also monotonically decreased with increasing POD_0 (Fig 2B; POD_0: $P < 0.001$). However, the other effects were non-significant, probably as a consequence of lower stomatal conductance (g_w) and an earlier g_w drop in the 100 ppb O_3 treatment (S2A Fig) causing low POD_0 differences between the two treatments (S2B Fig).

Structural evolution of HR-like lesions proceeded independent of O_3 exposure or leaf position

Dead cells within HR-like lesions showed *post-mortem* evolution of their cellular ultrastructure. Using leaf cross-sections *versus* disc samples (Fig 3E and 3F *versus* 1B inset), HR-like lesions in the CF + 100 ppb O_3 treatment were detected after 13 *versus* 8 days of exposure, once the leaf percentage area of lesions at both leaf positions was close to 10% (Table 1, Fig 1 and S1 Fig). The first HR-like lesions were observed in the lower palisade parenchyma. At an early developmental stage (stage 1), cell death was indicated by cell cytorrhysis, in apparent causal link with vacuole collapse, segmentation and tonoplast rupture (Fig 3E and 3F). This initiation of cell content disruption occurred before any alteration evidence in the surrounding organelle structure could be observed. At an intermediate stage of HR-like reaction development (stage 2), the organelles became increasingly disrupted, the cytoplasm condensed, and the cell integrity was lost (Fig 3G–3K'). Several hallmarks of oxidative stress and HR-like reactions (Table 1) became apparent, such as (1) degradation of the mitochondrial matrix and envelope (Fig 3H), (2) nucleus pyknosis (Fig 3I), (3) chloroplast disruption (Fig 3J), and (4) leakage of cellular debris into the apoplast through cell wall breaks (Fig 3K and 3K'). In the final stage of HR-like reaction development (stage 3), the cell content appeared completely disrupted, with amorphous remnants–except starch grains–densely fused together (Fig 3L–3N). The surrounding living cells showed local cell wall thickening, following callose deposition on the cell wall portion adjacent to dead HR-like cells (Fig 3O and 3P). These three stages of HR-like reaction development and their markers (Table 1) could be

Fig 1. Development dynamics of non-oxidized and oxidized HR-like lesions at the 3rd leaf position in hybrid poplar (*Populus tremula x alba*), **as a function of O_3 treatment and time.** {model: lmer[log(variable+1) ~ leaf position * Oxidation * Time * O_3 treatment + (1|pot)]; *** $P \leq 0.001$; * $P \leq 0.05$}. The inset image is a synthetic image of the particle distribution and morphology in each lesion color class (non-oxidized/oxidized) during image analyses of HR-like reactions. Values represent percentage area means ± SE of leaf discs showing non-oxidized or oxidized HR-like lesions (n = 4). Different letters indicate significant differences between treatments at a given assessment date (Tukey's honestly significant difference (HSD) post-hoc test, $P \leq 0.05$).

https://doi.org/10.1371/journal.pone.0282006.g001

observed within adjacent cells or cell groups scattered in the lower or upper palisade parenchyma layer. The HR-like stages and cell ultrastructure showed similar characteristics, irrespective of O_3 treatment, leaf position and exposure duration (13, 23 days), with apparent *post-mortem* evolution.

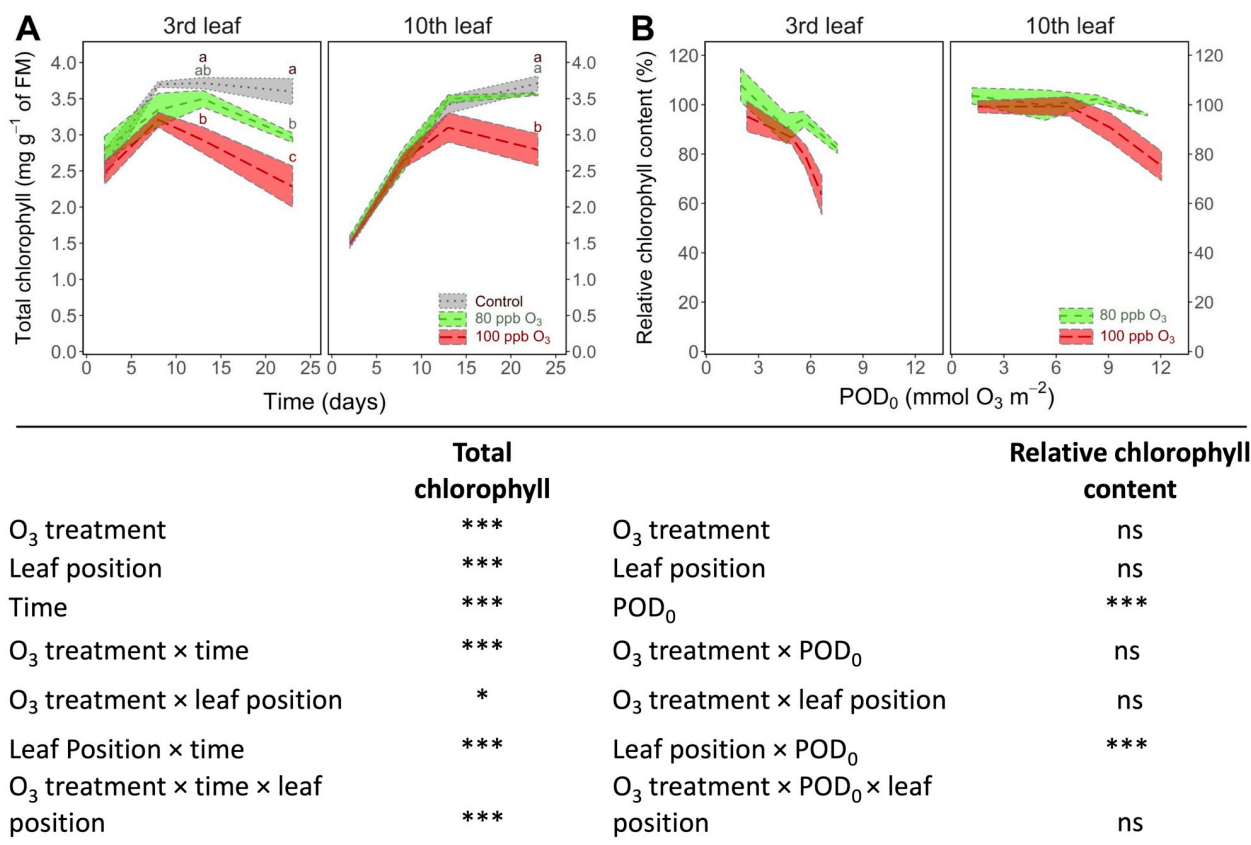|	Total chlorophyll		Relative chlorophyll content
O_3 treatment	***	O_3 treatment	ns
Leaf position	***	Leaf position	ns
Time	***	POD_0	***
O_3 treatment × time	***	O_3 treatment × POD_0	ns
O_3 treatment × leaf position	*	O_3 treatment × leaf position	ns
Leaf Position × time	***	Leaf position × POD_0	***
O_3 treatment × time × leaf position	***	O_3 treatment × POD_0 × leaf position	ns

Fig 2. Dynamics of changes in the total chlorophyll concentration within leaves of hybrid poplar (*Populus tremula x alba*) as a function of assessment time (A; mg g^{-1} of fresh matter), POD_0 (B; percentage of values in the CF treatment). O_3 treatment (dotted line: CF, dashed line: CF +80 ppb O_3, long dash line: CF +100 ppb O_3), leaf position, and their interactions (model: lmer(variable ~ O_3 treatment * leaf position * time or POD_0 + (1 | tree/chamber)); *** $P \leq 0.001$, * $P \leq 0.05$, ns not significantly different). Values represent means ± SE (n = 4). Different letters indicate significant differences between treatments on a given assessment date (post-hoc Tukey's HSD, $P \leq 0.05$).

Ultrastructural traits showed degenerative dynamics at least partly determined by O_3 exposure and leaf position

Mesophyll cells surrounding the HR-like lesions showed typical structural and ultrastructural markers of ACS in response to the O_3 treatments. These injuries represented an obvious aggravation and acceleration of ontological senescence processes observed in CF material of comparable age (Fig 4K–4O and 4P–4T *versus* Fig 4A–4E and 4F–4J; Table 1). At the cellular level, the injuries included a relative increase in vacuome size at the expense of cytoplasm and an apparent reduction in the number and size of chloroplasts (Fig 4K, 4L, 4P and 4Q *versus* Fig 4A, 4B, 4F and 4G). At the subcellular level, we observed (1) cell wall thickening (Fig 5), (2), various degenerative changes (poor thylakoid membrane resolution following oxidative injury (Fig 4R and 4T *versus* Fig 4M and 4O); increase in plastoglobuli size and frequency (Fig 4G, 4H, 4Q and 4R, versus Fig 4B, 4C, 4L and 4M)) and larger starch grains in chloroplasts (Fig 4K–4M and 4P–4R *versus* Fig 4A–4C and 4F–4H), (3) missing nucleoli indicative of lower nuclear transcription activity (Fig 4N and 4S *versus* Fig 4D and 4I), and (3) accumulation of secondary metabolites in the vacuole (Fig 4P *versus* Fig 4F). The ACS-related changes became apparent after 13 days of treatment (Table 1). Until the end of the experiment, they appeared more severe in the 100 ppb O_3 treatment and at the 3rd leaf position. Cell wall thickening processes were specific to leaf position: at
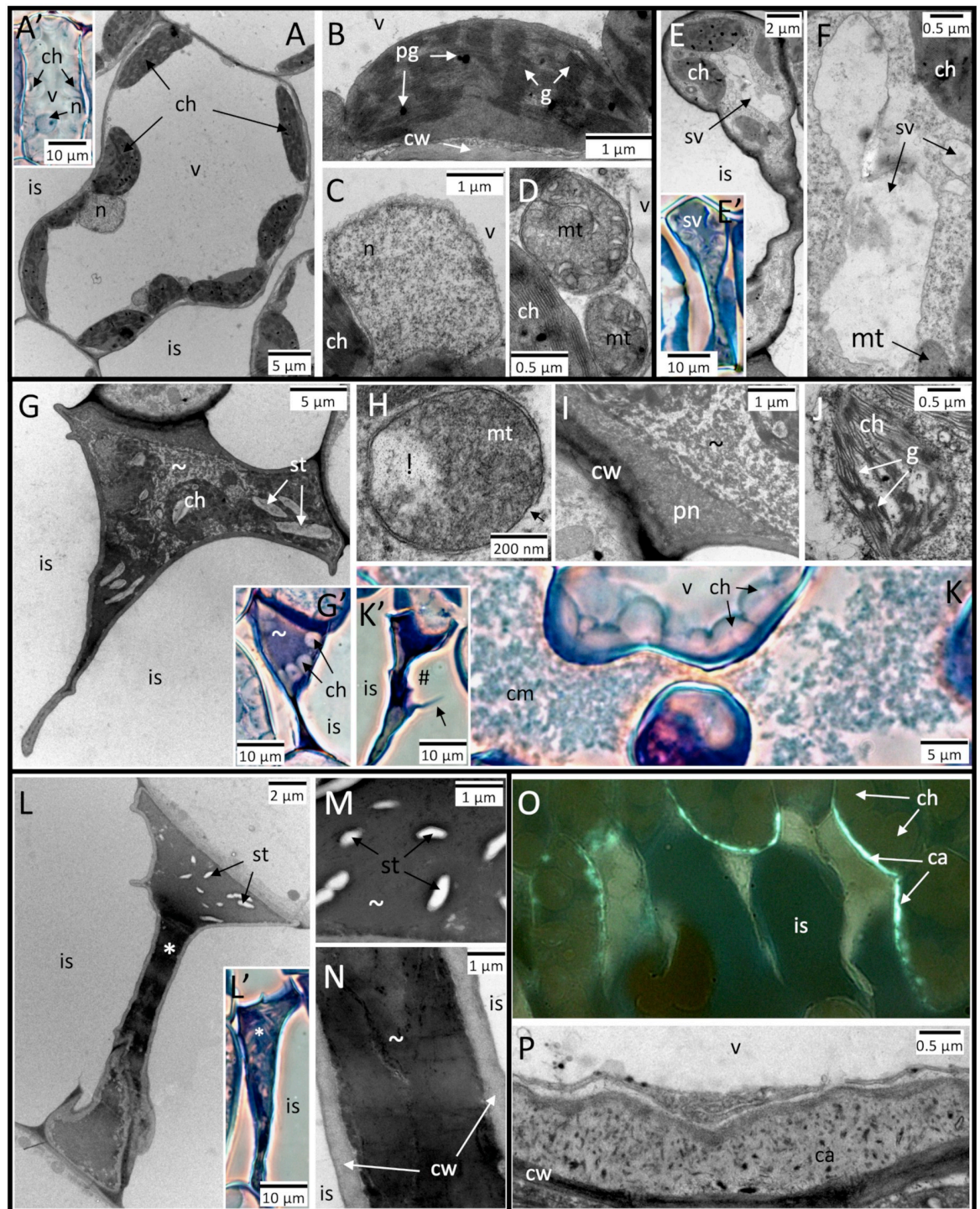
Fig 3. Evolution of cellular and subcellular traits in HR-like lesions within mesophyll cells of hybrid poplar (*Populus tremula x alba*) leaves at the 3rd (A–D, K–P) and 10th leaf position (E–J) and in response to the CF+100 ppb O₃ treatment. **A–D** Asymptomatic mesophyll cell structure in the CF treatment. **E–F** Early stage of HR-like reaction development: cell death and cytorrhysis. In apparent relation to cell cytorrhysis, the vacuole was shrunken (sv) and its irregular shape indicated tonoplast rupture, whereas other organelles were still intact. **G–K** Intermediate stage of HR-like reaction development: disruption of cell content. **H** Within mitochondria, degradation of the mitochondrial matrix (!) and disruption of outer membrane (arrow). **I** Nucleus pyknosis (pn) and condensation of cytoplasm (~). **J** chloroplast (ch) disruption. **K–K'** Leakage of cell debris (cm) into the intercellular space (is) through break points in the cell wall (#). **L–N** Final stage of HR-like reaction development: condensation and fusion of cellular debris. **O–P** Local thickening of cell wall (cw) through callose deposition within cells adjacent to lesions. Other structures: g: grana, n: nucleus, v: vacuole. Technical specifications: post-fixation

using OsO4; contrasting using uranyl acetate and lead citrate; observation in TEM (**A, B–E, F, G, H-J, L, M, N, P**); staining with Toluidine blue and observation under phase contrast in bright field microscopy (**A', E', G'-K', L'**); staining with Aniline blue and observation with fluorescence microscopy (**O**).

the 3rd leaf position, multivesicular bodies discharged degraded cellular remnants into the periplasm by exocytosis, while little physiological activity could be observed in the cytoplasm (Fig 5A–5C, Table 1). At the 10th leaf position, dense networks within the cytoplasm of (1) burgeoning rough endoplasmic reticulum, (2) dictyosomes, with their trans domains and the secreted vesicles oriented towards cell walls, and (3) numerous mitochondria all indicated ontological cell wall thickening processes, together with cellulose microfibril deposition (Fig 5D–5G, Table 1).

Chloroplast traits were responsive to changes in the O_3 exposure and showed a clear evolution over time, with significant differences between the mesophyll layers. Primarily the

Table 1. Development of structural and ultrastructural markers of O_3 stress over 30 days of exposure to the CF +100 ppb O_3 and CF +80 ppb O_3 treatment *versus* CF treatment, within the mesophyll of hybrid poplar leaves (*Populus x tremula alba*).

Compartment	Structural marker	Physiological process	Experimental factors									Fig.
			Treatment	100 ppb O_3						80 ppb O_3		
			Leaf position	3rd			10th			3rd	10th	
			Exposure (*days*)	8	13	23	8	13	23	13	13	
Leaf blade	Leakage of cellular material into apoplast	HR-like		+	-	-	-	+	-	-	-	3K
Cell	Cytorrhysis	HR-like		-	+	+	-	+	+	+	-	3G and 3L
	Rupture of cell wall	HR-like		-	-	+	+	-	+	+	-	3K'
	Disruption of cell content											
	Rupture of membrane (plasmalemma and tonoplast)	HR-like		-	+	+	-	+	+	+	-	3E–3F
	Disruption of organelles	HR-like		-	+	+	-	+	+	-	-	3H and 3J
	Condensation of cellular debris	HR-like		-	-	+	+	-	+	+	+	3L–3N
	Cell wall thickening											
	Wart-like protrusion	Oxidative stress		-	-	+	-	-	+	-	-	Not shown
	Discharge of autophagic vacuoles	ACS		-	-	+	-	-	-	-	-	5A
	Cell wall synthesis	Leaf ontology		-	+	+	+	+	+	-	-	5D–5G,
	Callose deposition	HR-like		-	+	+	-	-	+	-	-	3O and 3P
Cytoplasm	Autophagy	ACS		-	-	+	-	-	-	-	-	5B and 5C
	Condensation	ACS		-	+	+	-	+	+	-	-	not shown
Vacuole	Size increase	ACS		-	+	+	-		+	+	-	4Q vs 4G
	Collapse	HR-like		-	+	+	-	+	+	+	-	3F
	Accumulation of secondary product in the vacuole	Oxidative stress ACS		-	+	+	-	-	+	-	-	4P
Nucleus	Picnosis	HR-like		-	+	-	-	-	-	-	-	3I
	Condensation	ACS			-	+	-	-	+	-	-	4S
Chloroplast	Size decrease	ACS		-	+	+	-	-	+	-	-	6
	Increase in size and density of plastoglobuli	ACS		-	+	+	-	+	+	+	-	4R and 4T vs 4M and 4O
	Higher circularity	ACS		-	-	+	-	-	+	-	-	6
	Disruption	HR-like		-	+	+	-	+	+	+	-	3J
Mitochondria	Disruption	Oxidative stress		-	+	+	-	+	+	+	+	3H

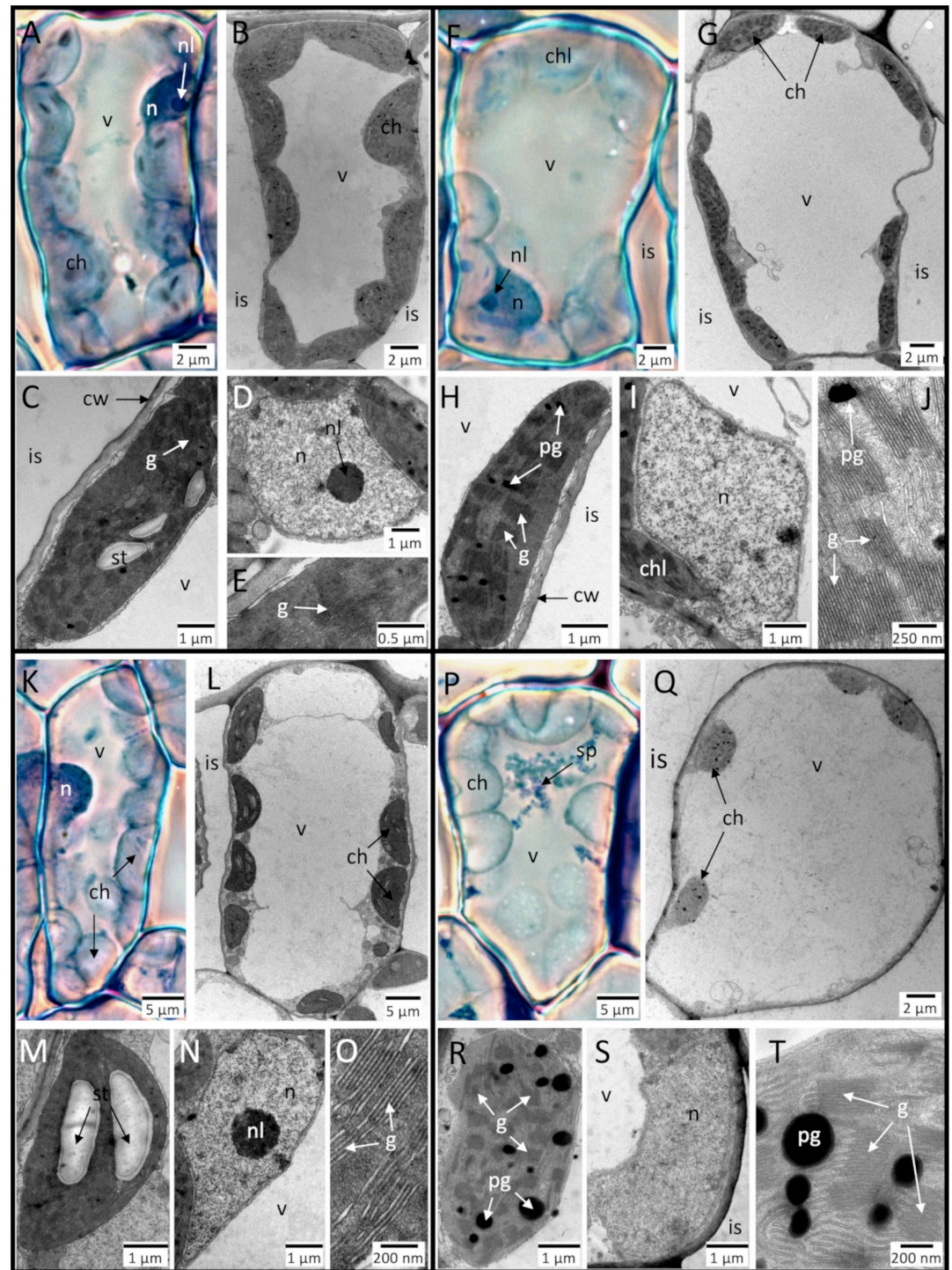"+" and "-" indicates presence and absence of marker, respectively.

Fig 4. Evolution of degenerative traits at the cellular and subcellular level within mesophyll cells surrounding HR-like lesions inside of hybrid poplar (*Populus tremula x alba*) leaves at the 3rd leaf position and in response to the CF+100 ppb O_3 (K–O, P–T) treatment relative to the CF treatment (A–E, F–J). Treatment time: 8 days (**A–E, K–O**) or 23 days (**F–J, P–T**). The main difference between the two treatments was the quicker evolution of degenerative traits in the O_3-treated trees (**F, G**) relative to the CF trees (**P, Q**). Markers at the cellular level: relative increase in vacuole (v) size at the expense of cytoplasm and the apparent reduction in the number and size of chloroplasts (ch). Markers at the subcellular level: within chloroplasts: increase in starch grain (st) accumulation (**K–M** *vs.* **A–C**), injury to thylakoid membranes of grana (g; **R, T** *vs.* **H, J**) and increase in the plastoglobuli (pg) size and frequency (**Q, R,** *vs.* **G, H**); within nucleus (n): condensation of chromatin and loss of nucleoli (nl; **N, S** *vs.* **D, I**); in the vacuole: accumulation of secondary metabolites (sp; **P** *vs.* **F**). Other structures: cw: cell wall, is: intercellular space. Technical specifications: post-fixation using OsO_4, contrasting using uranyl acetate and lead citrate, observation in TEM (**B–E, G–J, L–O, Q–T**); staining with Toluidine blue, observation under phase contrast in bright field microscopy (**A, F, K, P**).
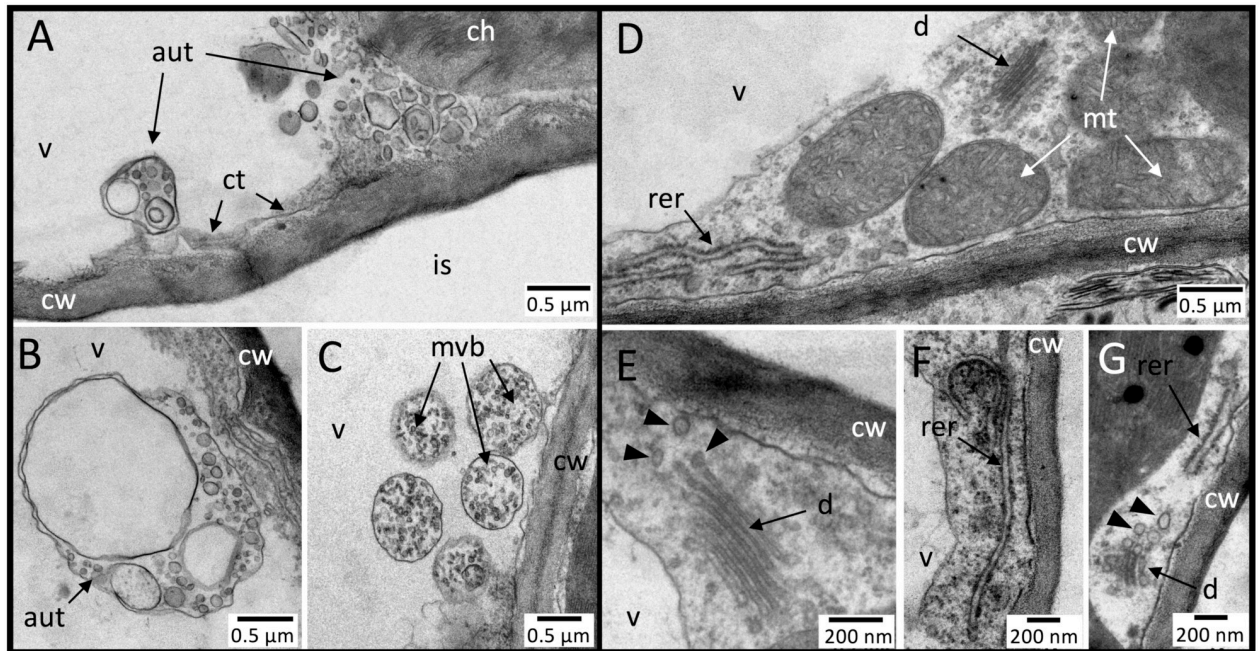
Fig 5. Contrast in the cell wall thickening processes at the 3rd (A–C) *vs.* 10th leaf position (D–G) within leaf mesophyll cells undergoing ACS processes from hybrid poplar (*Populus tremula x alba*) trees in the CF+100 ppb O_3 treatment. A–C At the 3rd leaf position, cell wall thickening primarily resulted from exocytosis (~) of multivesicular body (mvb) content into the periplasm (pe), as a consequence of autophagic processes. Notice the thin cytoplasm (ct) layer and few organelles. **D–G** At the 10th leaf position, ontological cell wall thickening in response to treatment was indicated by a dense network of mitochondria (mt; **D**), rough endoplasmic reticulum (rer; **F**), and dictyosomes (d; **E**) secreting vesicles (arrowheads in **E**, **G**) heading towards apoplast. Other structures: ch: chloroplast, cw: cell wall, is: intercellular space, v: vacuole. Technical specifications: post-fixation using OsO_4, contrasting using uranyl acetate and lead citrate, observation in TEM.

https://doi.org/10.1371/journal.pone.0282006.g005

chloroplast shape (circularity) and the total plastoglobuli area were affected by the O_3 treatment and increasing POD_0 (Fig 6; $P < 0.001$). By the end of the exposure in the 100 ppb O_3 *versus* CF treatment, the plastoglobuli area was 10-fold larger and the chloroplast circularity had increased by 40%, irrespective of leaf position (Fig 6, S1 Table; O_3 treatment*time: $P < 0.001$). As indicated by significant effects of leaf position ($P < 0.001$) and time ($P < 0.001$, plastoglobuli only), these two parameters also responded to ontological developmental processes, which O_3 exposure accelerated (O_3 treatment or POD_0*leaf position: $P < 0.05$). Chloroplasts in the lower palisade parenchyma layer tended to be rounder (Fig 6, S1 Table; mesophyll layer: $P < 0.001$). Chloroplast size decreased over time ($P < 0.001$), most likely corresponding to foliar phenological development, but it was not responsive to O_3 treatment and POD_0. Starch grain size and abundance responded to apparent chloroplast illumination and foliar phenology, as indicated by significant effects of leaf position, time, mesophyll layer and their interactions (Fig 6; $P < 0.01$). Comparing the 100 *versus* 80 ppb O_3 treatment on one assessment date (13 days of O_3 exposure), the findings appeared rather similar and the sensitivity of plastoglobuli to oxidative stress was further confirmed (S3 Fig; O_3 treatment and POD_0: $P < 0.001$).

Discussion

Contrasts between HR-like and ACS dynamics

In confirmation of Turc, Vollenweider [18], sigmoid-like and monotonic plant response dynamics appeared to be characteristic of HR-like and ACS processes within foliage under O_3
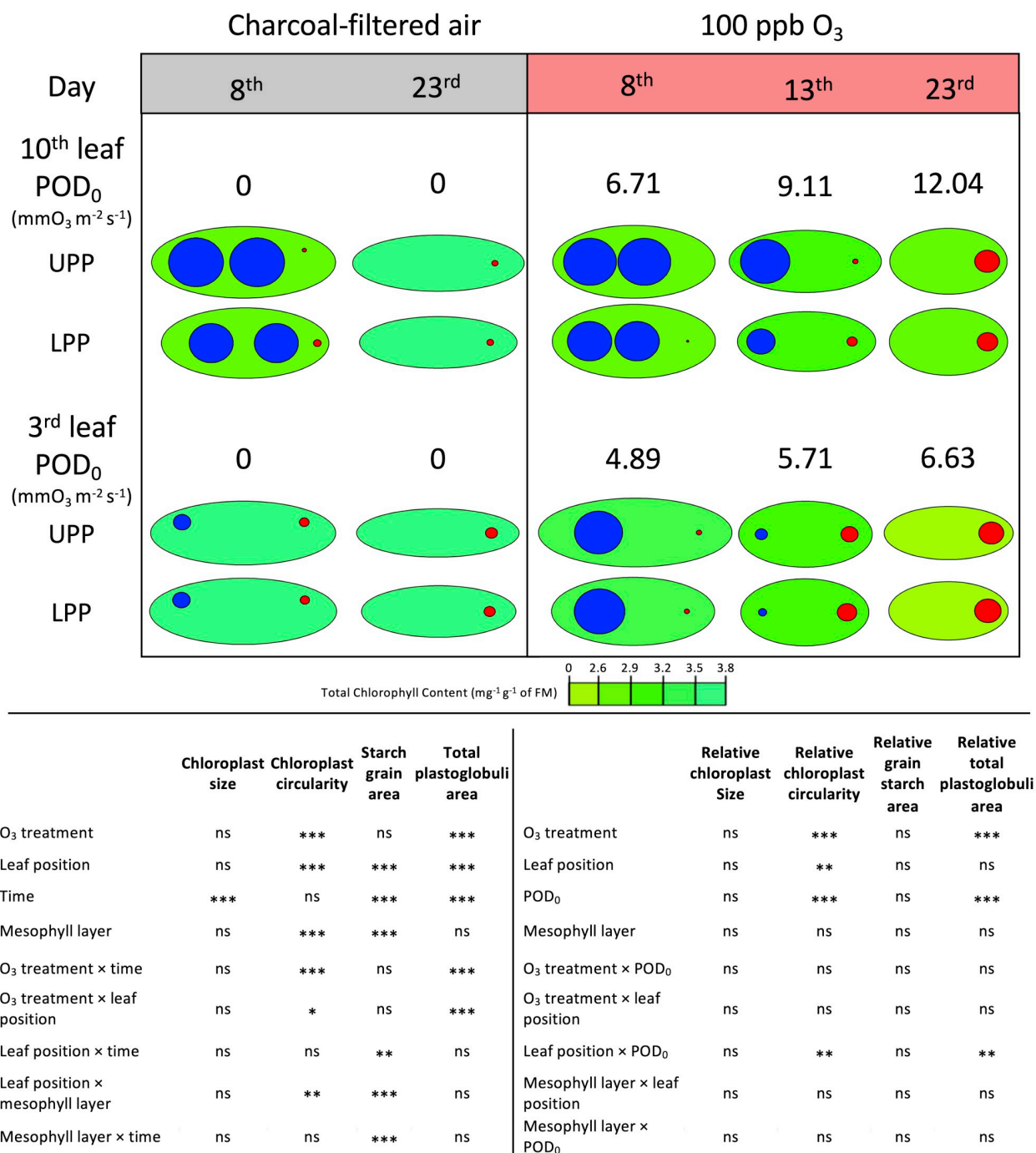
Fig 6. Visualization of chloroplast size and shape trait dynamics as a function of O_3 treatment, leaf position, assessment time or POD_0, mesophyll layer, and interactions, as observed in the leaf mesophyll of hybrid poplar trees (*Populus tremula x alba*) on the 8th, 13th and 23rd day of treatment. Model: lmer(variable ~ O_3 treatment * leaf position * time + (1 | cell/tree)); *** $P \leq 0.001$, * $P \leq 0.05$, ns not significantly different). Data basis for the conceptual models of chloroplast trait changes: chloroplast long and short axis (green ellipse), cumulated starch grain and plastoglobuli percentage area (blue and red circles), total chlorophyll content (in mg g^{-1} FM; green color scale).

stress. In this replicated experiment, the HR-like reactions and their dynamics at the different leaf positions matched quite well with those previously observed [18]. The duration of the latency period and plateau values were strikingly similar in the two experiments, irrespective of treatment and leaf position. However, the beginning of degenerative reactions was different when the total chlorophyll content was assessed rather than the reflectance. Although reflectance-based has been shown to be one of the best ways to measure chlorophyll content without destroying plants [55, 56], in our study the assessment method appeared important, with the biochemical assay being more accurate and specific to chlorophylls than reflectance-based estimates. Nevertheless, the dynamics of the ACS plant response appeared little affected by the assessment method, with the results from this replicated experiment overall matching quite well those obtained previously.

While rather monotonic degenerative responses to O_3 stress have been observed in various studies [23, 57, 58], experimental confirmation of the sigmoid-like dynamics in the case of HR-like lesions has been missing so far, instead remaining an implicit hypothesis based on apoptosis science [59, 60]. As cell death is the earliest event during HR-like lesion development, its selection as the structural marker being monitored allowed us to sensitively and comprehensively assess HR-like events and dynamics. The numerous other, more specific apoptosis markers were found to appear afterwards, during the *post-mortem* ontological development of the lesion. This is the first time, to our knowledge, that structural injury resulting from HR-like processes has been shown to develop in dead cells and thus without biological control. Some of the released cell debris–notably from cell walls–may act as signals within the surrounding tissues [61, 62]. The three observed stages of HR-like reaction development may correspond to an injury severity scale or result from successive degradation of dead cell contents. Arguments in favor of the former interpretation include (1) the occurrence of all three stages during the first observation of HR-like reactions and (2) the occurrence of all three stages within the same cell in some cases, with part of the cell still in disruption and the rest with fused remnants (*i.e.*, Fig 3G). The argument that the stages of HR-like reaction development are successive primarily rely on the concept of delayed lesion oxidation, which increases over time [18]. The non-oxidized HR-like lesions appeared to correspond to cells in the first stage of HR-like reaction development, as organelles were not disrupted but rather intact, as indicated by the presence of chlorophyll [18]. Since oxidized lesions had a disrupted cell content, the cellular material in stage 3 and at least part of that in stage 2 should be included in the oxidized lesion class during quantitative assessments.

Callose deposits on cell walls as a consequence of O_3 exposure form a typical HR-like marker [21, 36, 63], which was observed within mesophyll cells adjacent to lesions in poplar leaves. They are also found in the case of plant–pathogen interactions and hypersensitive responses (HR), strengthening cell walls and slowing pathogen-induced damage [64]. Callose deposition is promoted by salicylic acid and suppressed by jasmonic acid [65], and the observed deposition pattern may result from interacting effects of both hormones [66].

Whilst occurring at an early stage of HR-like injury, ACS represented a terminal programmed cell death (PCD) event, which had not yet been completed in material analyzed in LM and TEM. Dynamics of ACS-related changes proceeded as a coordinated decrease in apparent cellular activity and chlorophyll content concomitant with various subcellular degenerative changes, especially inside of chloroplast. Similar traits were observed during autumnal senescence in other species, such as rice [67], Scots pine [68] and beech [48]. In the case of beech, plastoglobuli were larger and displayed more intense extrusion to the vacuole than in poplar. It suggests a larger degree of lipid remobilization processes in the former species, which might be associated with beech competitive and shade-tolerance traits [69].

Two chloroplast traits, namely circularity and total plastoglobuli area, were particularly responsive to O_3 treatment and POD_0. They also showed alteration with leaf aging and thus responded in a way similar to total chlorophyll content. Taken together, the measured traits indicated injury to thylakoids and pointed the chloroplast inner membrane system as being particularly sensitive to oxidative stress [70]. During senescence, decreased antioxidant capacities in chloroplasts trigger ROS production, resulting in a feedback loop accelerating the senescence process [71]. O_3 stress, and high levels of photo-oxidative stress observed in the field [19], may contribute to further accelerating the degenerative processes. The chloroplast size and starch grain accumulation responded to leaf aging and chloroplast illumination only, while they were not affected by O_3 treatment or dose.

Leaf-age-mediated responses to O_3 stress

A reduction in total chlorophyll content, emergence of HR-like lesions, and ACS-related microscopic changes occurred later and with a larger POD_0 at the 10th versus 3rd leaf position, consistent with a higher tolerance of developing leaves [37, 39, 72]. Being observed at both leaf positions, the cell wall thickening activity proceeded in a different way, depending on the ontological development reached at each foliage level. At the lower leaf position, cell wall thickening was promoted by autophagic processes, in direct association with the degeneration of cellular content. The tolerance gained thus appears uncertain, and such processes may even contribute to accelerated leaf shedding, as observed during experimental exposure of mature non-acclimated foliage to O3 [23, 73]. In top leaves, cell wall thickening proceeded as during cell growth. This latter process is adaptative [74] and implies tight transcriptional regulation of ROS homeostasis [42, 75], which may help in coping with additional O_3-induced ROS. The two thickening processes thus appeared to be functionally related to lower (3rd leaf position) versus enhanced (10th leaf position) O_3 tolerance. They are consistent with observed increase in stress susceptibility during sink-to-source transition in maturing foliage [76]. Further supporting this idea, the ACS-related changes in O_3-exposed foliage of tested poplar trees started once the sink-to-source transition had apparently been achieved, as indicated by the plateau reached in chlorophyll content and stomatal conductance within the CF trees.

Leaf response and visible injury dynamics

Macroscopic injury, used in risk assessment studies [31–33], represents a terminal reaction resulting from different types of structural injury, with specific dynamics and plant responses proceeding at different paces. With only the oxidized HR-like lesions contributing to stippling-like visible injury [18], a significant fraction of disruptive processes may remain undetected, at least at an early stage of symptom development. As a consequence, the rapidity and extent of structural responses to O_3 stress appear to be generally underestimated. Cell death detection in less controlled experimental conditions may lack specificity. ACS-related changes, which responded sensitively to increasing POD_0 in our study, have a similar limitation. In multi-stress situations, quantitative or observational assessments should therefore rely on a combination of markers. As assessments are generally completed late during the vegetation season and rarely repeated, the observed injury should be considered the cumulative result of multiple events, depending on each response occurring before the sampling date [19]. This finding may provide the principal explanation for the spatial and temporal variability in visible injury observed in field conditions.

Conclusion

In this study, we investigated the dynamics of structural and ultrastructural changes occurring in poplar leaves in response to two O_3 levels and as a function of time, phytotoxic O_3 dose (POD_0), leaf developmental stage, and mesophyll layer. Although the development dynamic of HR-like lesions depended on O_3 concentration and POD_0, most of the HR-like structural and ultrastructural markers appeared after cell death, independent of the experimental factors. By contrast, the pace of degenerative ACS processes was closely depending on the O_3 levels, POD_0 and leaf development. At the subcellular level, thylakoid membranes in chloroplasts were identified as being one of the most sensitive subcellular structures to O_3 stress. Concerning our experimental hypotheses (H), structural injury developed in parallel with physiological and biochemical reactions in the case of ACS but not HR-like reactions (partial rejection of H1). Dynamics of HR-like and ACS responses, as well as structural markers, were response-specific (confirmation of H2), with cellular reactions being the same at the 3rd and 10th leaf positions, except cell wall thickening processes (partial confirmation of H3). Finally, dynamics of ACS responses in leaves with different leaf ontological progress differed over time and with POD_0 (confirmation of H4). With specific markers and contrasted dynamics, ACS and HR-like processes appear fairly independent, which provide a rationale for observed variability in the symptom display. A combination of easily assessed ACS and HR-like markers, such as chlorophyll reflectance and mesophyll cell death, appears best suited for specifically quantifying O_3 effects in trees during *e.g.* risk assessment studies. In a time of rapid climate change and given the varying interplay of HR-like and ACS processes with environmental conditions, an open question is how foliar responses to O_3 stress may evolve in the future.

Supporting information

S1 Fig. Development dynamics of non-oxidized and oxidized HR-like lesions at the 10th leaf position in hybrid poplar (*Populus tremula x alba*) as a function of O_3 treatment and time. {model: lmer[log(variable+1) ~ leaf position * oxidation * time * O_3 treatment + (1|pot)]; *** $P \leq 0.001$; * $P \leq 0.05$}.}. The inset image is a synthetic image of the particle distribution and morphology in each lesion color class (non-oxidized/oxidized) during image analyses of HR-like reactions. Values represent percentage area means ± SE of leaf discs showing non-oxidized or oxidized HR-like lesions (*n* = 4). Different letters indicate significant differences between treatments at a given assessment date (Tukey's honestly significant difference post-hoc test, $P \leq 0.05$).
(TIFF)

S2 Fig. Dynamics of changes in the (A) stomatal conductance to water (g_w) and (B) phytotoxic O_3 dose (POD_0) of hybrid poplar leaves (*Populus tremula x alba*) as a function of O_3 treatment (CF ●, CF+80 ppb O_3 ▲, CF+100 ppb O_3 ■), leaf position and time of assessment. {model: lmer[sqrt(variable)] ~ O_3 treatment * leaf position * time + (1 | tree/chamber); ***$P \leq 0.001$}. Values represent means ± SE (n = 4). Different letters indicate significant differences between treatments for a given assessment date (Tukey's honestly significant difference post-hoc test, $P \leq 0.05$).
(TIFF)

S3 Fig. Dynamics of size and shape changes in chloroplast traits as a function of O_3 treatment, leaf position, POD_0, mesophyll layer and interactions, as observed in the leaf mesophyll of hybrid poplar trees (*Populus tremula x alba*) on the 13th day of treatment. Model: lmer(variable ~ O_3 treatment * leaf position * POD_0 + (1 | cell/tree)); *** $P \leq 0.001$, * $P \leq 0.05$, ns not significantly different). Green ellipse: chloroplast, blue circle: total starch grain area, red

circle: total plastoglobuli area. Green shading represents the total chlorophyll content (mg g^{-1} of FM).
(TIFF)

S1 Table. Evolution of chloroplast size and shape in the leaf mesophyll of hybrid poplar trees (*Populus tremula* x *alba*) in response to O_3 treatment, leaf position, mesophyll layer and assessment time. Values represent mean ± SE, n = 4. Different letters indicate significant differences between treatments for a given assessment date (Tukey's honestly significant difference post-hoc test, $P \leq 0.05$). (model implemented in R: lmer(variable ~ O_3 treatment * leaf position * time + mesophyll layer +(1 | cell/tree)).
(DOCX)

Acknowledgments

Author Contributions

Conceptualization: Benjamin Turc, Yves Jolivet, Mireille Cabané, Marcus Schaub, Pierre Vollenweider.

Data curation: Benjamin Turc.

Formal analysis: Benjamin Turc.

Funding acquisition: Yves Jolivet, Mireille Cabané, Marcus Schaub, Pierre Vollenweider.

Investigation: Benjamin Turc.

Methodology: Benjamin Turc, Pierre Vollenweider.

Supervision: Yves Jolivet, Mireille Cabané, Pierre Vollenweider.

Visualization: Benjamin Turc.

Writing – original draft: Benjamin Turc.

Writing – review & editing: Benjamin Turc, Yves Jolivet, Mireille Cabané, Marcus Schaub, Pierre Vollenweider.

References

1. Lefohn AS, Malley CS, Smith L, Wells B, Hazucha M, Simon H, et al. Tropospheric ozone assessment report: Global ozone metrics for climate change, human health, and crop/ecosystem research. Elementa-Science of the Anthropocene. 2018; 6. https://doi.org/10.1525/elementa.279 PMID: 30345319

2. Monks PS, Archibald AT, Colette A, Cooper O, Coyle M, Derwent R, et al. Tropospheric ozone and its precursors from the urban to the global scale from air quality to short-lived climate forcer. Atmospheric Chemistry and Physics. 2015; 15(15):8889–973. https://doi.org/10.5194/acp-15-8889-2015

3. Jiang JH, Aksoyoglu S, Ciarelli G, Baltensperger U, Prevot ASH. Changes in ozone and PM2.5 in Europe during the period of 1990–2030: Role of reductions in land and ship emissions. Science of the Total Environment. 2020; 741. https://doi.org/10.1016/j.scitotenv.2020.140467 PMID: 32886963

4. Simon H, Reff A, Wells B, Xing J, Frank N. Ozone trends across the United States over a period of decreasing NOx and VOC emissions. Environmental Science & Technology. 2015; 49(1):186–95. https://doi.org/10.1021/es504514z PMID: 25517137

5. Chang KL, Petropavlovskikh I, Cooper OR, Schultz MG, Wang T. Regional trend analysis of surface ozone observations from monitoring networks in eastern North America, Europe and East Asia. Elementa-Science of the Anthropocene. 2017; 5. https://doi.org/10.1525/elementa.243

6. Gaudel A, Cooper OR, Ancellet G, Barret B, Boynard A, Burrows JP, et al. Tropospheric Ozone Assessment Report: Present-day distribution and trends of tropospheric ozone relevant to climate and global atmospheric chemistry model evaluation. Elementa-Science of the Anthropocene. 2018; 6. https://doi.org/10.1525/elementa.291

7. Lu X, Zhang L, Wang XL, Gao M, Li K, Zhang YZ, et al. Rapid increases in warm-season surface ozone and resulting health impact in China since 2013. Environmental Science and Technology Letters. 2020; 7(4):240–7. https://doi.org/10.1021/acs.estlett.0c00171

8. Feng ZZ, Kobayashi K. Assessing the impacts of current and future concentrations of surface ozone on crop yield with meta-analysis. Atmospheric Environment. 2009; 43(8):1510–9. https://doi.org/10.1016/j.atmosenv.2008.11.033

9. Mills G, Sharps K, Simpson D, Pleijel H, Broberg M, Uddling J, et al. Ozone pollution will compromise efforts to increase global wheat production. Global Change Biology. 2018; 24(8):3560–74. https://doi.org/10.1111/gcb.14157 PMID: 29604158

10. Pleijel H, Broberg MC, Uddling J, Mills G. Current surface ozone concentrations significantly decrease wheat growth, yield and quality. Science of the Total Environment. 2018; 613:687–92. https://doi.org/10.1016/j.scitotenv.2017.09.111 PMID: 28938211

11. Li P, Feng ZZ, Catalayud V, Yuan XY, Xu YS, Paoletti E. A meta-analysis on growth, physiological, and biochemical responses of woody species to ground-level ozone highlights the role of plant functional types. Plant Cell and Environment. 2017; 40(10):2369–80. https://doi.org/10.1111/pce.13043 PMID: 28744869

12. Proietti C, Anav A, De Marco A, Sicard P, Vitale M. A multi-sites analysis on the ozone effects on gross primary production of European forests. Science of the Total Environment. 2016; 556:1–11. https://doi.org/10.1016/j.scitotenv.2016.02.187 PMID: 26971205.

13. Wittig VE, Ainsworth EA, Naidu SL, Karnosky DF, Long SP. Quantifying the impact of current and future tropospheric ozone on tree biomass, growth, physiology and biochemistry: a quantitative meta-analysis. Global Change Biology. 2009; 15(2):396–424. https://doi.org/10.1111/j.1365-2486.2008.01774.x

14. Sacchelli S, Carrari E, Paoletti E, Anav A, Hoshika Y, Sicard P, et al. Economic impacts of ambient ozone pollution on wood production in Italy. Sci Rep. 2021; 11(1). https://doi.org/10.1038/s41598-020-80516-6 PMID: 33420285

15. Kerstiens G, Lendzian KJ. Interactions between ozone and plant cuticles. 1. Ozone deposition and permeability. New Phytologist. 1989; 112(1):13–9. https://doi.org/10.1111/j.1469-8137.1989.tb00303.x

16. Laisk A, Kull O, Moldau H. Ozone concentration in leaf intercellular air dpaces is close to zero. Plant Physiology. 1989; 90(3):1163–7. https://doi.org/10.1104/pp.90.3.1163 PMID: 16666867

17. Mills G., Harmens H., Hayes F., Pleijel H., Buker P., I. G. Mapping critical levels for vegetation. Manual on methodologies and criteria for Modelling and mapping critical loads and levels and air pollution effects, Risks and Trends. International Cooperative Programme on Effects of Air Pollution on Natural Vegetation and Crops. 2017:1–66. https://www.researchgate.net/publication/329101282_MAPPING_CRITICAL_LEVELS_FOR_VEGETATION_Revised_Chapter_3_of_the_Manual_on_Methodologies_and_Criteria_for_Modelling_and_Mapping_Critical_Loads_and_Levels_and_Air_Pollution_Effects_Risks_and_Trends/citations.

18. Turc B, Vollenweider P, Le Thiec D, Gandin A, Schaub M, Cabane M, et al. Dynamics of Foliar Responses to O3 Stress as a Function of Phytotoxic O3 Dose in Hybrid Poplar. Frontiers in Plant Science. 2021; 12. https://doi.org/10.3389/fpls.2021.679852 PMID: 34262582

19. Vollenweider P, Günthardt-Goerg MS, Menard T, Baumgarten M, Matyssek R, Schaub M. Macro- and microscopic leaf injury triggered by ozone stress in beech foliage (*Fagus sylvatica* L.). Annals of Forest Science. 2019; 76(3):71. https://doi.org/10.1007/s13595-019-0856-5

20. Bussotti F, Agati G, Desotgiu R, Matteini P, Tani C. Ozone foliar symptoms in woody plant species assessed with ultrastructural and fluorescence analysis. New Phytologist. 2005; 166(3):941–55. https://doi.org/10.1111/j.1469-8137.2005.01385.x PMID: 15869654

21. Feng G, Calatayud V, García-Breijo F, Reig-Armiñana J, Feng Z. Effects of elevated ozone on physiological, anatomical and ultrastructural characteristics of four common urban tree species in China. Ecological Indicators. 2016; 67:367–79. https://doi.org/10.1016/j.ecolind.2016.03.012

22. Guerrero CC, Günthardt-Goerg MS, Vollenweider P. Foliar symptoms triggered by ozone stress in irrigated holm oaks from the city of Madrid, Spain. PLoS ONE. 2013; 8(7). https://doi.org/10.1371/journal.pone.0069171 PMID: 23894424

23. Moura BB, Alves ES, Marabesi MA, de Souza SR, Schaub M, Vollenweider P. Ozone affects leaf physiology and causes injury to foliage of native tree species from the tropical Atlantic Forest of southern

Brazil. Science fo the Total Environment. 2018; 610:912–25. https://doi.org/10.1016/j.scitotenv.2017.08.130 PMID: 28830051

24. Vollenweider P, Fenn ME, Menard T, Günthardt-Goerg M, Bytnerowicz A. Structural injury underlying mottling in ponderosa pine needles exposed to ambient ozone concentrations in the San Bernardino Mountains near Los Angeles, California. Trees. 2013; 27(4):895–911. https://doi.org/10.1007/s00468-013-0843-7

25. Pasqualini S, Piccioni C, Reale L, Ederli L, Della Torre G, Ferranti F. Ozone-induced cell death in tobacco cultivar Bel W3 plants. The role of programmed cell death in lesion formation. Plant Physiology. 2003; 133(3):1122–34. https://doi.org/10.1104/pp.103.026591 PMID: 14612586.

26. Schraudner M, Moeder W, Wiese C, Van Camp W, Inze D, Langebartels C, et al. Ozone-induced oxidative burst in the ozone biomonitor plant, tobacco Bel W3. Plant Journal. 1998; 16(2):235–45. https://doi.org/10.1046/j.1365-313x.1998.00294.x PMID: 22507138

27. Rao MV, Davis KR. The physiology of ozone induced cell death. Planta. 2001; 213(5):682–90. https://doi.org/10.1007/s004250100618 PMID: 11678271

28. Sandermann H. Molecular ecotoxicology of plants. Trends in Plant Science. 2004; 9(8):406–13. https://doi.org/10.1016/j.tplants.2004.06.001 PMID: 15296863

29. Günthardt-Goerg MS, Vollenweider P. Linking stress with macroscopic and microscopic leaf response in trees: new diagnostic perspectives. Environmental Pollution. 2007; 147(3):467–88. https://doi.org/10.1016/j.envpol.2006.08.033 PMID: 17050053.

30. Pell EJ, Sinn JP, Brendley BW, Samuelson L, Vinten-Johansen C, Tien M, et al. Differential response of four tree species to ozone-induced acceleration of foliar senescence. Plant Cell and Environment 1999; 22(7):779–90. https://doi.org/10.1046/j.1365-3040.1999.00449.x

31. Gerosa G, Marzuoli R, Rossini M, Panigada C, Meroni M, Colombo R, et al. A flux-based assessment of the effects of ozone on foliar injury, photosynthesis, and yield of bean (Phaseolus vulgaris L. cv. Borlotto Nano Lingua di Fuoco) in open-top chambers. Environmental Pollution. 2009; 157(5):1727–36. https://doi.org/10.1016/j.envpol.2008.06.028 PMID: 18657889

32. Sicard P, De Marco A, Dalstein-Richier L, Tagliaferro F, Renou C, Paoletti E. An epidemiological assessment of stomatal ozone flux-based critical levels for visible ozone injury in Southern European forests. Science of the Total Environment. 2016; 541:729–41. https://doi.org/10.1016/j.scitotenv.2015.09.113 PMID: 26437347

33. Sicard P, Hoshika Y, Carrari E, De Marco A, Paoletti E. Testing visible ozone injury within a Light Exposed Sampling Site as a proxy for ozone risk assessment for European forests. J For Res. 2021; 32 (4):1351–9. https://doi.org/10.1007/s11676-021-01327-7

34. Bussotti F, Schaub M, Cozzi A, Krauchi N, Ferretti M, Novak K, et al. Assessment of ozone visible symptoms in the field: perspectives of quality control. Environmental Pollution. 2003; 125(1):81–9. https://doi.org/10.1016/s0269-7491(03)00095-2 PMID: 12804830

35. Schaub M, Calatayud V. Assessment of Visible Foliar Injury Induced by Ozone. Forest Monitoring: Methods for Terrestrial Investigations in Europe with an Overview of North America and Asia. Developments in Environmental Science. 122013. p. 205–21.

36. Paoletti E, Contran N, Bernasconi P, Gunthardt-Goerg MS, Vollenweider P. Structural and physiological responses to ozone in Manna ash (Fraxinus ornus L.) leaves of seedlings and mature trees under controlled and ambient conditions. Science of the Total Environment. 2009; 407(5):1631–43. https://doi.org/10.1016/j.scitotenv.2008.11.061 PMID: 19136142

37. Paakkonen E, Metsarinne S, Holopainen T, Karenlampi L. The ozone sensitivity of birch (*Betula pendula*) in relation to the developmental stage of leaves. New Phytologist. 1996; 132(1):145–54. https://doi.org/10.1111/j.1469-8137.1996.tb04520.x PMID: 33863056

38. Zhang J, Schaub M, Ferdinand JA, Skelly JM, Steiner KC, Savage JE. Leaf age affects the responses of foliar injury and gas exchange to tropospheric ozone in *Prunus serotina* seedlings. Environmental Pollution. 2010; 158(8):2627–34. https://doi.org/10.1016/j.envpol.2010.05.003 PMID: 20537450.

39. Bagard M, Le Thiec D, Delacote E, Hasenfratz-Sauder MP, Banvoy J, Gerard J, et al. Ozone-induced changes in photosynthesis and photorespiration of hybrid poplar in relation to the developmental stage of the leaves. Physiologia Plantarum. 2008; 134(4):559–74. https://doi.org/10.1111/j.1399-3054.2008.01160.x PMID: 18823329.

40. Reich PB. Effects of low concentrations of O3 on net photosynthesis, dark respiration, and chlorophyll contents in aging hybrid poplar leaves. Plant Physiology. 1983; 73(2):291–6. https://doi.org/10.1104/pp.73.2.291 PMID: 16663210

41. Strohm M, Eiblmeier M, Langebartels C, Jouanin L, Polle A, Sandermann H, et al. Responses of transgenic poplar (*Populus tremula x P-alba*) overexpressing glutathione synthetase or glutathione reductase to acute ozone stress: visible injury and leaf gas exchange. J Exp Bot. 1999; 50(332):365–74. https://doi.org/10.1093/jxb/50.332.365

42. Mangano S, Juarez SPD, Estevez JM. ROS regulation of polar growth in plant cells. Plant Physiology. 2016; 171(3):1593–605. https://doi.org/10.1104/pp.16.00191 PMID: 27208283

43. Lichtenthaler H. Chlorophylls and Carotenoids: Pigments of Photosynthetic Biomembranes. Methods in Enzymology. 1987; 148.

44. Porra RJ, Thompson WA, Kriedemann PE. Determination of accurate extinction coefficients and simultaneous-equations for assaying chlorophyll-a and chlorophyll-B extracted with 4 different solvents—verification of the concentration of chlorophyll standards by atomic-absorption spectroscopy. Biochimica Et Biophysica Acta. 1989; 975(3):384–94. https://doi.org/10.1016/S0005-2728(89)80347-0

45. Bagard M, Jolivet Y, Hasenfratz-Sauder MP, Gerard J, Dizengremel P, Le Thiec D. Ozone exposure and flux-based response functions for photosynthetic traits in wheat, maize and poplar. Environ Pollut. 2015; 206:411–20. https://doi.org/10.1016/j.envpol.2015.07.046 PMID: 26253315

46. Feder N, Obrien TP. Plant microtechnique—some principles and new methods. American Journal of Botany. 1968; 55(1):123-+. https://doi.org/10.2307/2440500

47. Gerlach D. Botanische Mikrotechnik. Stuttgart: Thieme Verlag ed1984.

48. Mikkelsen TN, Heide-Jørgensen HS. Acceleration of leaf senescence in *Fagus sylvatica* L by low levels of tropospheric ozone demonstrated by leaf colour, chlorophyll fluorescence and chloroplast ultrastructure. Trees-Structure and Function. 1996; 10(3):145–56.

49. Pell EJ, Schlagnhaufer CD, Arteca RN. Ozone-induced oxidative stress: Mechanisms of action and reaction. Physiologia Plantarum. 1997; 100(2):264–73. https://doi.org/10.1034/j.1399-3054.1997.1000207.x

50. Schindelin J, Arganda-Carreras I, Frise E, Kaynig V, Longair M, Pietzsch T, et al. Fiji: an open-source platform for biological-image analysis. Nature Methods. 2012; 9(7):676–82. https://doi.org/10.1038/nmeth.2019 PMID: 22743772

51. Lemon J. Plotrix: a package in the red light district of R. R-News. 2006; 6(4):8–12.

52. R Development Core Team. R: A language and environment for statistical computing. Vienna, Austria: R Foundation for Statistical Computing; 2017.

53. Bates D, Machler M, Bolker BM, Walker SC. Fitting linear mixed-effects models using lme4. Journal of Statistical Software. 2015; 67(1):1–48. https://doi.org/10.18637/jss.v067.i01

54. Lenth RV. Least-Squares Means: The R Package lsmeans. Journal of Statistical Software. 2016; 69 (1):1–33. https://doi.org/10.18637/jss.v069.i01

55. Alam MS, Maina AW, Feng Y, Wu L-B, Frei M. Interactive effects of tropospheric ozone and blast disease (Magnaporthe oryzae) on different rice genotypes. Environmental Science and Pollution Research. 2022; 29(32):48893–907. https://doi.org/10.1007/s11356-022-19282-z PMID: 35201578

56. Ashrafuzzaman M, Lubna FA, Holtkamp F, Manning WJ, Kraska T, Frei M. Diagnosing ozone stress and differential tolerance in rice (Oryza sativa L.) with ethylenediurea (EDU). Environmental Pollution. 2017; 230:339–50. https://doi.org/10.1016/j.envpol.2017.06.055 PMID: 28668595

57. Gravano E, Bussotti F, Strasser RJ, Schaub M, Novak K, Skelly J, et al. Ozone symptoms in leaves of woody plants in open-top chambers: ultrastructural and physiological characteristics. Physiologia Plantarum. 2004; 121(4):620–33. https://doi.org/10.1111/j.1399-3054.2004.00363.x

58. Tresmondi F, Alves ES. Structural changes in Psidium guajava 'Paluma' leaves exposed to tropospheric ozone. Acta Botanica Brasilica. 2011; 25(3):542–8.

59. Alvarez ME, Pennell RI, Meijer PJ, Ishikawa A, Dixon RA, Lamb C. Reactive oxygen intermediates mediate a systemic signal network in the establishment of plant immunity. Cell. 1998; 92(6):773–84. https://doi.org/10.1016/s0092-8674(00)81405-1 PMID: 9529253

60. Levine A, Pennell RI, Alvarez ME, Palmer R, Lamb C. Calcium-mediated apoptosis in a plant hypersensitive disease resistance response. Current Biology. 1996; 6(4):427–37. https://doi.org/10.1016/s0960-9822(02)00510-9 PMID: 8723347

61. Benedetti M, Pontiggia D, Raggi S, Cheng ZY, Scaloni F, Ferrari S, et al. Plant immunity triggered by engineered in vivo release of oligogalacturonides, damage-associated molecular patterns. Proc Natl Acad Sci U S A. 2015; 112(17):5533–8. https://doi.org/10.1073/pnas.1504154112 PMID: 25870275

62. Koziel E, Otulak-Koziel K, Bujarski JJ. Plant cell wall as a key player during resistant and susceptible plant-virus interactions. Frontiers in Microbiology. 2021; 12. https://doi.org/10.3389/fmicb.2021.656809 PMID: 33776985

63. Vollenweider P, Ottiger M, Günthardt-Goerg MS. Validation of leaf ozone symptoms in natural vegetation using microscopical methods. Environmental Pollution. 2002; 124(1):101–18. https://doi.org/10.1016/s0269-7491(02)00412-8 PMID: 12683987

64. Wang Y, Li XF, Fan BF, Zhu C, Chen ZX. Regulation and function of defense-related callose deposition in plants. Int J Mol Sci. 2021; 22(5). https://doi.org/10.3390/ijms22052393 PMID: 33673633

65. Yi SY, Shirasu K, Moon JS, Lee SG, Kwon SY. The activated SA and JA signaling pathways have an influence on flg22-triggered oxidative burst and callose deposition. PLoS ONE. 2014; 9(2). https://doi.org/10.1371/journal.pone.0088951 PMID: 24586453

66. Kangasjarvi J, Jaspers P, Kollist H. Signalling and cell death in ozone-exposed plants. Plant Cell and Environment. 2005; 28(8):1021–36. https://doi.org/10.1111/j.1365-3040.2005.01325.x

67. Inada N, Sakai A, Kuroiwa H, Kuroiwa T. Senescence program in rice (Oryza sativa L.) leaves: analysis of the blade of the second leaf at the tissue and cellular levels. Protoplasma. 1999; 207(3–4):222–32. https://doi.org/10.1007/BF01283003

68. Kivimaeenpaeae M, Sutinen S. Microscopic structure of Scots pine (Pinus sylvestris (L.)) needles during ageing and autumnal senescence. Trees-Structure and Function. 2007; 21(6):645–59. https://doi.org/10.1007/s00468-007-0157-8

69. Arni D, Gricar J, Jevsenak J, Bozic G, von Arx G, Prislan P. Different wood anatomical and growth responses in european beech (Fagus sylvatica L.) at three forest sites in Slovenia. Frontiers in Plant Science. 2021; 12. https://doi.org/10.3389/fpls.2021.669229 PMID: 34381473

70. Lichtenthaler H. Plastoglobuli, Thylakoids, Chloroplast Structure and Development of Plastids. In: Biswal B, Krupinska K, Biswal U, editors. Plastid Development in Leaves during Growth and Senescence: Springer; 2013. p. 337–61.

71. Mayta ML, Hajirezaei MR, Carrillo N, Lodeyro AF. Leaf senescence: the chloroplast connection comes of age. Plants-Basel. 2019; 8(11). https://doi.org/10.3390/plants8110495 PMID: 31718069

72. Strohm M, Eiblmeier M, Langebartels C, Jouanin L, Polle A, Sandermann H, et al. Responses of antioxidative systems to acute ozone stress in transgenic poplar (*Populus tremula* x *P-alba*) over-expressing glutathione synthetase or glutathione reductase. Trees-Structure and Function. 2002; 16(4–5):262–73. https://doi.org/10.1007/s00468-001-0157-z

73. Günthardt-Goerg MS, McQuattie CJ, Scheidegger C, Rhiner C, Matyssek R. Ozone-induced cytochemical and ultrastructural changes in leaf mesophyll cell walls. Canadian Journal of Forest Research. 1997; 27(4):453–63. https://doi.org/10.1139/x96-187

74. Knox JP. Revealing the structural and functional diversity of plant cell walls. Current Opinion in Plant Biology. 2008; 11(3):308–13. https://doi.org/10.1016/j.pbi.2008.03.001 PMID: 18424171

75. Schmidt R, Kunkowska AB, Schippers JHM. Role of reactive oxygen species during cell expansion in leaves. Plant Physiology. 2016; 172(4):2098–106. https://doi.org/10.1104/pp.16.00426 PMID: 27794099

76. Coleman JS. Leaf development and leaf stress: increased susceptibility associated with sink-source transition. Tree Physiology. 1986; 2(1–3):289–99. https://doi.org/10.1093/treephys/2.1-2-3.289 PMID: 14975862